MRL-R-919

AR-003-901

DEPARTMENT OF DEFENCE

DEFENCE SCIENCE AND TECHNOLOGY ORGANISATION

MATERIALS RESEARCH LABORATORIES

MELBOURNE, VICTORIA

AD-A160 759

REPORT

MRL-R-919

COMPUTER AIDED AMMUNITION RADIOGRAPHY

K.K.M. Wu, J.D. Quinn and
D.F. Hedger

DTIC
EL
OCT 3 1 1985
A

"Original contains color
plates: All DTIC reproduct-
ions will be in black and
white"

Approved for Public Release

MRL

DTIC FILE COPY

85
2

DEPARTMENT OF DEFENCE

MATERIALS RESEARCH LABORATORIES

REPORT

MRL-R-919

COMPUTER AIDED AMMUNITION RADIOGRAPHY

K.K.M. Wu, J.D. Quinn and
D.F. Hedger

ABSTRACT

A need exists for improving the current methods for ensuring the safety of ammunition fuzes. Accordingly the feasibility of using automatic techniques for the inspection of ammunition fuzes has been investigated. The investigation covered the following aspects. (1) The usefulness of image enhancement techniques for the improvement of the detectability of defects; (2) the feasibility of automatic recognition of defects: and (3) the merits and the practicability of using real-time radiography to replace the film-based system for fuze inspection. It may be concluded from the feasibility study that image qualities can be significantly enhanced for visual detection. When a defect can be characterised in terms of the intensity and geometrical factors of its radiographic images automatic identification of the defect also appears to be feasible. The assessment also indicated that the use of real-time radiography is now a practical proposition.

Approved for Public Release

QUALITY
INSPECTED
5

DOCUMENT CONTROL DATA SHEET

REPORT NO.	AR NO.	REPORT SECURITY CLASSIFICATION
MRL-R-919	AR-003-901	UNCLASSIFIED

TITLE

Computer aided ammunition radiography

AUTHOR(S)	CORPORATE AUTHOR
K.K.M. Wu, J.D. Quinn and D.F. Hedger	Materials Research Laboratories P.O. Box 50, Ascot Vale, Victoria 3032

REPORT DATE	TASK NO.	SPONSOR
JULY 1985	DST 82/143	DSTO

CLASSIFICATION/LIMITATION REVIEW DATE	CLASSIFICATION/RELEASE AUTHORITY
	Superintendent, MRL Physics Division

SECONDARY DISTRIBUTION

Approved for Public Release

ANNOUNCEMENT

Announcement of this report is unlimited

KEYWORDS

Radiography	Ammunition	Pattern recognition
Fuzes (ordnance)	Inspection Defects	Image processing

COSATI GROUPS	1402	1901

ABSTRACT

        A need exists for improving the current methods for ensuring the
safety of ammunition fuzes. Accordingly the feasibility of using automatic
techniques for the inspection of ammunition fuzes has been investigated. The
investigation covered the following aspects. (1) The usefulness of image
enhancement techniques for the improvement of the detectability of defects; (2)
the feasibility of automatic recognition of defects: and (3) the merits and the
practicability of using real-time radiography to replace the film-based system
for fuze inspection. It may be concluded from the feasibility study that image
qualities can be significantly enhanced for visual detection. When a defect can
be characterised in terms of the intensity and geometrical factors of its
radiographic images automatic identification of the defect also appears to be
feasible. The assessment also indicated that the use of real-time radiography
is now a practical proposition.

C O N T E N T S

COMPUTER AIDED AMMUNITION RADIOGRAPHY

1.   INTRODUCTION

The hazards presented by premature detonation of ammunition
resulting from defective fuzes is a major concern to the Services. It is
proposed that an automatic inspection system based on computer image
enhancement and pattern recognition can provide improved fuze safety and
quality assurance. This can be achieved by reducing the current reliance on
error prone human inspection of radiographs. The feasibility of such a system
operating on radiographic images has been established. The investigation
addressed three facets of the problem: (1) the usefulness of image
enhancement techniques for the improvement of the detectability of defects;
(2) the feasibility of automatic recognition of defects; and (3) the merits
and the practicability of a photoelectronic digital (PEDI) imaging system to
replace the film-based system for fuze inspection. The work was performed
under the sponsorship of the Australian Ordnance Council.

2.   MACHINE IMAGE ENHANCEMENT AND RECOGNITION

2.1 Description of Input Images

The investigation was based on two sets of radiographs supplied by
the Munitions Filling Factory, St. Marys. Each set of radiographs consisted
of images of seven naval fuzes No. 259 N4. Six of the fuzes were modified to
contain one of six critical defects - defects which may cause premature
detonation of the fuze/parent projectile. The seventh fuze was a 'standard'
with all components present and correctly assembled. A cross-sectional
drawing of the standard is shown in Figure 1. Exposure details for the
radiographs were not available. However, it appears that all radiographs were
taken with similar X-ray exposure and geometry. Each fuze was positioned with
its axis at a right angle to the line of exposure, but not of fixed
orientation. In the second set of exposures, each fuze was rotated around its
axis to an orientation roughly 90° from the first set of exposures.

The defects incorporated into the fuzes were:

Fuze A - inverted arming ring

Fuze B - missing half collar

Fuze C - damaged safety ferrule

Fuze D - blunt striker point

Fuze E - missing shutter spring

Fuze F - detonator not fully screwed home

Drawings of the defects as seen on the radiographs and descriptions of the criteria used for visual examination of each defect are given in Figures 2 to 7.

2.2 Outline of Investigational Procedures

The X-ray photographic images were converted to 256 by 256 pixel (picture element) digital images using a Hamamatsu C1000-12 SIT closed circuit television camera. The intensity at each pixel was graded into one of 256 grey levels. The value 0 corresponds to the lowest intensity (black) and 255 corresponds to the highest intensity (white). A RAMTEK 9351 graphics system was used for image display. This system can generate up to 4096 colours on a colour monitor, and up to 256 grey levels on a monochrome monitor. An LSI 11/23 minicomputer was the host computer for the above systems, and handled the image processing and recognition. A block diagram of the entire system is given in Figure 8. A reproduction of the digital image of the standard as displayed on the monitor is shown in Figure 9. However, images of higher resolution, such as the close up view of the shutter assembly shown in Figure 10, were used for analyses.

It has been assumed during this preliminary study that all images can be normalised with respect to X-ray exposure, geometry and fuze orientation. This implies that images of a potentially defective component when being examined would be located at effectively the same area of the image frame and with similar intensity levels for all fuzes.

Two types of image enhancement techniques have been tried for improving image quality for visual inspection. The first technique involves the manipulation of intensity levels to highlight specific information. The second, displays the radiographic image in pseudo colour, so that small intensity differences may be displayed in highly contrasting colours instead of the normal grey levels. Automatic recognition of defects was based on the identification of characteristic grey level distribution and geometrical properties of the images. A list of computer programs developed for this investigation is given in the Annex.

Results of the study are given below.

2

2.3   Results of Investigation

2.3.1   Defect A - Inverted Arming Ring

Figure 11(a) shows an image of the section containing the arming ring of Fuze A (view 1) in which the arming ring is inverted. A similar section of the standard (view 1) is shown in Figure 11(b). Images of Fuze C,D,E and F are all similar to the standard. The two images have significant grey level differences in the regions both above the detonator and around the detonator as described in Figure 2 which enable visual identification to be made. Automatic recognition of this defect is feasible by basing the decision on average grey levels in selected regions above and around the detonator. The average intensity levels within a window of 45 x 80 pixels above the detonator, and a window of 60 x 60 pixels to the right of the detonator were measured. The values are listed in Table 1. For the two images of Fuze A, the average intensity of the window above the detonator is higher than that beside the detonator. But, for images of all other fuzes, the average intensity above the detonator is lower. Slight variations in the size and position of a window do not alter the readings significantly, as long as a window does not intrude into distinctly different regions.

The same two images displayed in colour are given in Figure 12, where intensities above a certain grey level threshold are displayed as red. The colour contrast and the distinct appearances of the red regions present a stronger set of image characteristics for visual identification. Automatic recognition of this defect may also be achieved through the determination of the size, shape and position of the centroid of the image displayed in red in Figure 12. Techniques for the analysis of geometrical properties of an image are described in detail in MRL Report No. 897.[1]

2.3.2   Defect B - Missing Half Collar

Images of the fuze section with a half collar missing (Fuze B) are shown in two orientations in Figure 13(a) & (b) with a corresponding view of the standard shown in Figure 13(c). View 1 of Fuze B is the preferred view for visual identification of the defect and is depicted in Figure 3. Identification is based on detecting the small grey level differences on the two sides of the striker. Digital image processing may be used to enhance the contrast of this part of an image. A histogram of the grey level distribution of the pixels inside the window is computed. The grey level range (g_1, g_2) within which the relevant information is concentrated can then be read from the histogram. The contrast of the image inside the window can be enhanced by stretching the levels in the range (g_1, g_2) to the whole range of 256 levels. This replaces the original grey level g of a pixel by g', where

$$g' = \frac{256}{g_2 - g_1} (g - g_1).$$

Results of this modification are illustrated in Figure 13. Visual identification of Fuze B is thus made possible with view 1. However, it is still not possible to identify this fault from view 2. This is because the

3

human eye can only differentiate approximately 32 grey levels, and thus is incapable of discriminating the relatively small intensity difference between these two images.

The images of Figure 13 are displayed in pseudo colour in Figure 15. The information inside the window, with intensities above an appropriately chosen threshold is displayed in yellow, while the rest is displayed in red. A threshold may be chosen enabling Fuze B to be identified from both view 1 and view 2 by the characteristic increase in red area when compared to the standard. It has also been established that images of Fuze C, D, E, F are all similar to that of the standard when displayed under the same colour scheme. The percentage of pixels with intensity in the range displayed in red for various images are given in Table 2. It appears that a fuze may be identified as defective or non-defective on the basis of whether this reading is greater or less than a decision boundary which may be estimated by a statistical classifier described in Section 3, (Figure 24). The readings in Table 2 depend upon the selected threshold level. With the exception of Fuze D view 2, the identification of all cases were not changed with threshold level variations of three grey levels from either side. Fuze D, view 2, would be correctly identified as non-defective when lower threshold values were used. The identifications, apart from the case of Fuze D view 2, were not altered with window displacements of one pixel in either the horizontal or the vertical directions. However, the effects of threshold selection and window registration on the identification requires more thorough investigation.

2.3.3 Defect C - Damaged Safety Ferrule

Images of the safety ferrule of Fuze C (view 1) and the standard are given in Figure 16. The damage is clearly visible. The detectability of this defect can be improved by enhancing the sharp transitions between adjacent regions. A common class of algorithm for detecting these transitions is based on the sequential examination of subareas for edges in a number of orientations. In general, edge element examination is carried out using subareas containing n^2 pixels in association with a template of the same size. For $n = 3$, the intensity levels for pixels contained in the examined subarea may be expressed as

$$C = \begin{matrix} c_{11} & c_{12} & c_{13} \\ c_{21} & c_{22} & c_{23} \\ c_{32} & c_{32} & c_{33} \end{matrix}$$

and the template may be expressed as

$$B = \begin{matrix} b_{11} & b_{12} & b_{13} \\ b_{21} & b_{22} & b_{23} \\ b_{32} & b_{32} & b_{33} \end{matrix}$$

4

Each pixel of the image to be processed, the element c_{22} of C, is replaced by the inner product of B and C.

$$(B, C) = \sum_{i=1}^{3} \sum_{j=1}^{3} b_{ij} c_{ij}$$

A combination of four templates has been used to enhance the edges of an image.[2] These are:

$$B_1 = \begin{array}{ccc} 1 & \sqrt{2} & 1 \\ 0 & 0 & 0 \\ -1 & -\sqrt{2} & -1 \end{array} \qquad\qquad B_2 = \begin{array}{ccc} 1 & 0 & -1 \\ \sqrt{2} & 0 & -\sqrt{2} \\ 1 & 0 & -1 \end{array}$$

$$B_3 = \begin{array}{ccc} 0 & -1 & \sqrt{2} \\ 1 & C & -1 \\ \sqrt{2} & 1 & 0 \end{array} \qquad\qquad B_4 = \begin{array}{ccc} \sqrt{2} & -1 & 0 \\ -1 & 0 & 1 \\ 0 & 1 & -\sqrt{2} \end{array}$$

which accentuates in turn edges in the horizontal, vertical and the two diagonal directions. The final enhanced edge is formed by combining the results of application of the four templates in the form

$$\left(\sum_{i=1}^{4} (B_i, C)^2 \right)^{1/2}.$$

The results are displayed in Figure 17. A suitable set of criteria for automatic recognition of this defect has yet to be formulated. It is envisaged that automatic recognition may be achieved through correlation of the enhanced edges of the two ferrules.

2.3.4 Defect D - Blunt Striker Point

Owing to the lack of details recorded on the original radiographs, no progress has been made with respect to this defect. Image enhancement techniques so far tried have all failed to improve the image quality sufficiently to reveal the necessary detail. This is clearly a case which calls for revised X-ray exposure.

5

2.3.5 Defect E - Missing Shutter Spring

The orientation of the shutter assembly was not referenced to the fuze when the two sets of radiographs were taken. The image of the spring is therefore only visible on some radiographs. Two images of the shutter assembly on which the spring is visible, are shown in Figure 18(a) and (b), and two images without the spring, the two views of Fuze E, are shown in Figure 18(c) and (d). Assuming that the orientation of the shutter assembly can be standardised during the X-ray exposure, all images of the spring would then have similar grey level readings lying within a narrow range. A small area in the vicinity of the spring has been processed to display all grey levels within this range inside this area in one colour, say yellow, and the rest is displayed in another colour, say red, as shown in Figure 19. The presence or absence of the spring may be identified automatically on recognition of the geometrical characteristics of the yellow images. Figure 20 shows the images of the area in the vicinity of the spring extracted from Figure 19. The two different cases: with spring ((a) and (c)) and without the spring ((b) and (d)), can be distinguished on the basis of the geometrical properties of the images (Table 3).

2.3.6 Defect F - Detonator Plug Not Fully Screwed Home

Sections of Fuze A, E, B, and F, showing parts of the shutter assembly, the detonator holder and the plug are shown in Figure 21. During the visual examination of radiographs, the defect is identified by the criterion described in Figure 7. The defective fuze is characterised by a diminished gap between the detonator plug and the shutter when compared with the standard. The region of interest is outlined by the window shown in Figure 21. Figure 22 shows these windows extracted from Figure 21 displayed i. colour. Intensities characterising the gap are displayed as purple. These windows are converted to binary images in Figure 23. Intensity levels representing the gap are displayed as white and all other levels are deemed to be background information and displayed as blue. Visual identification of the defect should be much easier from the binary images of Figure 23 than from the original images. Automatic recognition of the defect may be based upon the width and the normalised moment of inertia of the gap, which are listed in Table 4.

3. AUTOMATIC IDENTIFICATION OF DEFECTS

The ultimate objective of this study is to devise a system capable of identifying defective fuzes automatically in order to reduce the load of human inspection. The central issue is the practicability of designing a reliable scheme for the classification of information into different groups. In the present investigation, potentially defective components were examined one at a time. In each case a classifier capable of categorising patterns into one of two groups, the standard and the defective, is required. A suitable classifier for the current application is the Bayes classifier, which derives decision functions based upon the statistics of the measurements of

6

features categorising the groups. The main advantage of the Bayes classifier is that it can be trained rapidly. However, the decision functions are limited to a second degree system of equations which may not be sufficient for separation of patterns into more than two groups.

An object may be represented as a vector $\underline{x}$ formed by the set of n features categorising the pattern groups. Before an object has been measured, the only knowledge for classification available about the object is the a priori probabilities, $P(\omega_i)$ with i = 1 and 2, of the two pattern groups. However, the knowledge for classification can be increased with feature measurements $\underline{x}$ and the probability density function of the patterns $p(\underline{x}/\omega_i)$. According to Bayes theorem [3], the a posteriori probability that the object belongs to group ω_i is

$$P(\omega_i/\underline{x}) = \frac{p(\underline{x}/\omega_i)\, P(\omega_i)}{\sum\limits_{i=1}^{2} p(\underline{x}/\omega_i)P(\omega_i)}$$

Each object can then be assigned to the group with the higher $P(\omega_i/\underline{x})$. The decision threshold for the two class problem is that $\underline{x}$ which satisfies

$$p(\underline{x}/\omega_1)P(\omega_1) = p(\underline{x}/\omega_2)P(\omega_2) \ .$$

Feature measurements can be generally assumed to follow normal (Gaussian) distributions, and the corresponding probability density functions are of the form

$$p(\underline{x}/\omega_i) = \frac{1}{(2\pi)^{n/2}|\underline{C}_i|^{1/2}} \exp\left[-\frac{1}{2}(\underline{x}-\underline{m}_i)^T \underline{C}_i^{-1}(\underline{x}-\underline{m}_i)\right],$$

where $\underline{m}_i$ is the mean vector of the class ω_i and $\underline{C}_i$ is the covariance matrix. Thus the decision function is given by

$$\frac{P(\omega_1)}{|\underline{C}_1|^{1/2}} \exp\left[-\frac{1}{2}(\underline{x}-\underline{m}_1)^T \underline{C}_1^{-1}(\underline{x}-\underline{m}_1)\right] = \frac{P(\omega_2)}{|\underline{C}_2|^{1/2}} \exp\left[-\frac{1}{2}(\underline{x}-\underline{m}_2)^T \underline{C}_2^{-1}(\underline{x}-\underline{m}_2)\right],$$

or
$$\ln\frac{P(\omega_1)}{P(\omega_2)} - \frac{1}{2}\ln\frac{|\underline{C}_1|}{|\underline{C}_2|} - \frac{1}{2}\left[(\underline{x}-\underline{m}_1)^T\underline{C}_1^{-1}(\underline{x}-\underline{m}_1)-(\underline{x}-\underline{m}_2)^T\underline{C}_2^{-1}(\underline{x}-\underline{m}_2)\right] = 0.$$

The mean vectors and the covariance matrices may be estimated from a training set by the expressions:

$$\underline{m}_i = \frac{1}{N_i} \sum_{j=1}^{N_i} \underline{x}_{ij}$$

and

$$\underline{C}_i = \left[\frac{1}{N_i} \sum_{j=1}^{N_i} (\underline{x}_{ij} \cdot \underline{x}_{ij}^T)\right] - \underline{m}_i \underline{m}_i^T,$$

where $\underline{x}_{ij}$ is the jth sample from the group ω_i and N_i is the total number of samples in the training set belonging to group ω_i. The training set should consist of a sufficient number in each group to permit $\underline{m}_i$ and $\underline{C}_i$ to be computed with reasonable accuracy.

If the patterns are categorised by a single feature, the decision function is simply

$$\ln\frac{P(\omega_1)}{P(\omega_2)} - \ln\frac{\sigma_1}{\sigma_2} - \left[\frac{(x-\mu_1)^2}{2\sigma_1^2} - \frac{(x-\mu_2)^2}{2\sigma_2^2}\right] = 0$$

where μ_i and σ_i are respectively the mean and the standard deviation of x for patterns in group ω_i.

The method outlined above has been applied to the readings given in Tables 2 to 4, and the results are shown in Figures 24 to 26. These have been included as illustrative examples only, and are statistically invalid due to the small sample size. A much larger training set is needed to establish decision boundaries with high confidence.

For the current application, it is essential to bias the classification towards the group of defective fuzes in order to reduce the probability of mis-identifying a defective type as non-defective. This will increase the false alarms, but should be acceptable since further human inspection can clear these fuzes as non-defective. On the other hand, a missed identification of defective fuzes may lead to dire consequences. In the examples given in Figures 24 to 26, the decision boundaries were biased in favour of defective fuzes. This was achieved by allocating equal a priori probabilities to defective and non-defective fuzes, although in practice, the percentage of defective fuzes to be encountered during inspection would be very small. The effect on classification of various $P(\omega_1)/P(\omega_2)$ is illustrated in Figure 25.

The criterion adopted in the selection of features for categorising the groups is the variance normalized distance between the group means. For

8

feature x, this is given by

$$D_{12} = \frac{|\mu_1 - \mu_2|}{\sqrt{\sigma_1^2 + \sigma_2^2}}$$

The most useful choice is the feature which gives the greatest separation D_{12}. On this basis the width and the area normalised moment of inertia have been selected as the features for categorising Defect E. The third feature, the circularity - defined as 4π x area/perimeter^2, produces a much smaller D_{12}, and is not as useful for the identification of Defect E. (Table 3). The effectiveness of the feature descriptors and the resultant classifier need to be assessed through operational trials.

4.   PHOTOELECTRONIC DIGITAL IMAGING

Because of the complexity of the fuze, it is impossible to obtain an X-ray image which will reveal all features of interest with clear definition in a single exposure. Owing to this drawback the identification of some defects are difficult or impossible. Since the costs of film radiography are rising, the proposition of taking several exposures for each fuze is becoming less viable for a film-based system. On the other hand, the costs of PEDI imaging devices are falling and, at the same time, their qualities are rapidly improving. Equipments capable of producing X-ray images with qualities matching that of the film are now readily available. The performance of PEDI devices can be evaluated in terms of gain, resolution and dynamic range. Image intensifiers may be used to provide extremely high gain for the detection of X-rays down to single photon level. Hence an effective maximum useable gain is already available to radiographers using PEDI imaging. Resolution in the past was relatively low but with recent developments resolution above 2000 television lines is now available, which should be more than adequate for most applications. Dynamic range is another characteristic which has undergone dramatic improvement. Although the theoretical value of 4000 to 1 for radiographic films cannot be matched by PEDI, dynamic range of 1000 to 1 can be achieved with some high quality cameras, comparing fairly well with the limit of 2000 to 1 for most radiographs in practice.

A practical PEDI acquisition system can take one of the following forms:

(1)   X-ray image intensifier (XRII) plus CCTV camera

(2)   X-ray fluorescent screen plus low light level television (LLLTV) camera

(3)   X-ray proximity focused image intensifier plus CCTV camera

(4)   X-ray sensitive vidicon camera.

9

Method (1) can provide an optimal performance with respect to detection characteristics but its size is limited to a circular area of 300 mm diameter. Larger areas can be achieved by method (2) but with some loss in efficiency. Methods (3) and (4) are less commonly employed. The CCTV or LLLTV cameras of methods (1) to (3) can employ a variety of image sensor tube or, more recently solid state image sensor arrays. Presently a selection of image sensor tubes (e.g. vidicon, plumbicon, image isocon) are suitable for high quality real-time radiography. Solid state sensor arrays (e.g. charge coupled devices and addressable diode arrays) that are currently available have a low resolution and a variable sensitivity of individual sensor elements within an array. Further development is expected to overcome these problems whereupon the advantages of low voltage operation, shock resistance and small size will make solid state image sensors particularly suitable for hostile working environments. Their inherently flat array structure and data transfer methodology will also make them very amenable to computer processing of accurate geometric data.

PEDI systems can generate images in real- or near real-time with low running costs. These systems can individually examine potentially defective components under their optimum X-ray exposures. Another merit of the PEDI system is that its images can be stored much more compactly than films and are readily accessible. Therefore, it is believed that the PEDI system can be proven to be superior to the film-based system in terms of cost effectiveness, image quality and archival storage considerations. The PEDI system could also be adapted to gamma- and neutron-radiography.

5. CONCLUSIONS AND RECOMMENDATIONS

Pattern recognition and image processing techniques have been successfully applied to the inspection of critical defects of Naval Fuze No. 259 recorded on radiographs. In the present study it has been assumed that the image of each fuze component may be normalised with respect to X-ray exposure, geometry and orientation. This implies that the image of the particular component being examined would be located at the same part of the image frame, with similar intensity levels for all fuzes. It has been established during this investigation that image qualities could be enhanced for visual detection by the application of digital processing techniques and by the representation of radiographs in pseudo colour. When a defect can be successfully characterised in terms of intensity and/or geometrical factors, automatic detection is also possible. Furthermore, it is believed that the use of live PEDI images to replace images recorded on films is now technically feasible. A PEDI system is not only superior but also potentially more cost effective.

Further investigation is recommended in the following areas:

(1) Image enhancement and pattern recognition techniques should be extended to live X-ray images of Fuze 259. Images of potentially defective components should first be optimised individually for X-ray exposure, geometry and orientation. The objective would be to determine whether image qualities can be improved sufficiently to

10

reveal details not discernable from the existing radiographs, i.e. Defect D - the blunt striker point. An imaging system capable of storing and digitising an image in real-time or near real-time would be desirable. It should be capable of integrating a number of image frames for the improvement of signal noise ratio in cases where low signal levels occur. Such a system is now commercially available. An image intensifier may also be required for extremely low intensity application.

(2)   Techniques for automatically fixing the orientation of a fuze during exposure should be investigated. It is envisaged that the objective would be achieved through automatic recognition of prominent features of the fuze coupled with machine control of a robotic arm.

(3)   The feasibility of detection and identification of defects without a prior knowledge of the defects should be studied. This may be achieved by correlating images being examined with a standard. The normalisation of images with respect to exposure, geometry and orientation would be a prerequisite.

(4)   Application of this technique to the inspection of gamma- and neutron- radiographic images should be investigated.

        Finally, it is strongly recommended that an experimental PEDI X-radiography system be developed for operational trials which are essential to the design and evaluation of image processing and recognition algorithms. The system should be programmed to automatically recognise given defects, but at the same time should have facilities to display enhanced images for visual inspection, so that automatic system decisions can be verified by human inspectors.

6. REFERENCES

1. WU, K.K.M. (1983). "Automatic Mail Clearance Using Image Analysis."
       MRL-R-897.

2. Frei, W. and Chen, C.C. (1977). "Fast Boundary Detection and a New
       Algorithm." IEEE Trans. Comput., Vol. C-26, No. 10, pp. 988-998.

3. Castleman, K.R. (1979). "Digital Image Processing." Prentice-Hall,
       pp. 428

TABLE 1

Average intensity levels of the X-radiographic images of various fuzes within a window of 45 x 80 above the detonator and a window of 60 x 60 to the right of the detonator. These readings are used as the basis for the identification of Defect A.

Fuze		Average Intensity Level	
		Above Detonator (45 x 80)	Right of Detonator (60 x 60)
Standard	View 1	131	153
	View 2	133	169
Fuze C	View 1	133	160
	View 2	131	169
Fuze D	View 1	131	161
	View 2	126	167
Fuze E	View 1	130	158
	View 2	129	159
Fuze F	View 1	131	158
	View 2	135	165
Fuze A	View 1	159	147
	View 2	166	154

TABLE 2

Percentage of pixels with intensity below the threshold (information) displyed in red in Figure 13) for the X-radiographic images of the region corresponding to the safety collars. This value may be used as the basis for the identification of Defect B.

Fuze		Percentage of Pixels below Threshold
Standard View 1		25
	View 2	18
Fuze C	View 1	22
	View 2	25
Fuze D	View 1	30
	View 2	42
Fuze E	View 1	29
	View 2	15
Fuze F	View 1	25
	View 2	21
Fuze B	View 1	48
	View 2	59

TABLE 3

Geometrical properties of images extracted from a small area in the vicinity of the shutter spring (Figure 19). These readings may be used as the basis for the identification of Defect E.

Fuze		Area	Width	Circularity	Moment of Inertia (Area normalised)
Standard	View 1	228	14	0.348	0.258
Fuze A	View 1	201	13	0.387	0.255
	View 2	101	9	0.391	0.344
Fuze B	View 1	109	11	0.277	0.387
	View 2	165	11	0.325	0.274
Fuze C	View 1	140	10	0.392	0.328
Fuze D	View 1	155	9	0.380	0.291
Fuze F	View 2	187	13	0.379	0.295
Fuze E	View 1	104	6	0.342	0.659
	View 2	73	4	0.296	0.478
*Fuze C	View 1	85	7	0.269	0.693
*Fuze D	View 2	105	6	0.321	0.547

* Spring not visible due to unfavourable shutter orientation.

TABLE 4

Geometrical properties of the X-radiographic images of the gap between the detonator plug and the shutter (Figure 21) of various fuzes. These readings may be used as the basis for the identification of Defect F.

Fuze		Area	Width	Moment of Inertia (area normalised)
Standard	View 1	1715	23	0.669
	View 2	1573	19	0.739
Fuze A	View 1	1512	15	0.883
	View 2	1528	25	0.652
Fuze B	View 1	1491	24	0.650
	View 2	1185	13	1.059
Fuze C	View 1	1311	21	1.035
	View 2	937	10	1.381
Fuze D	View 1	1239	12	1.096
	View 2	1388	19	0.979
Fuze E	View 1	1569	16	0.922
	View 2	1866	18	0.714
Fuze F	View 1	383	9	2.450
	View 2	1018	13	1.416

Striker

Half collar

Safety ferrule

Detonator holder

Arming ring

Detonator plug

Shutter spring

Shutter
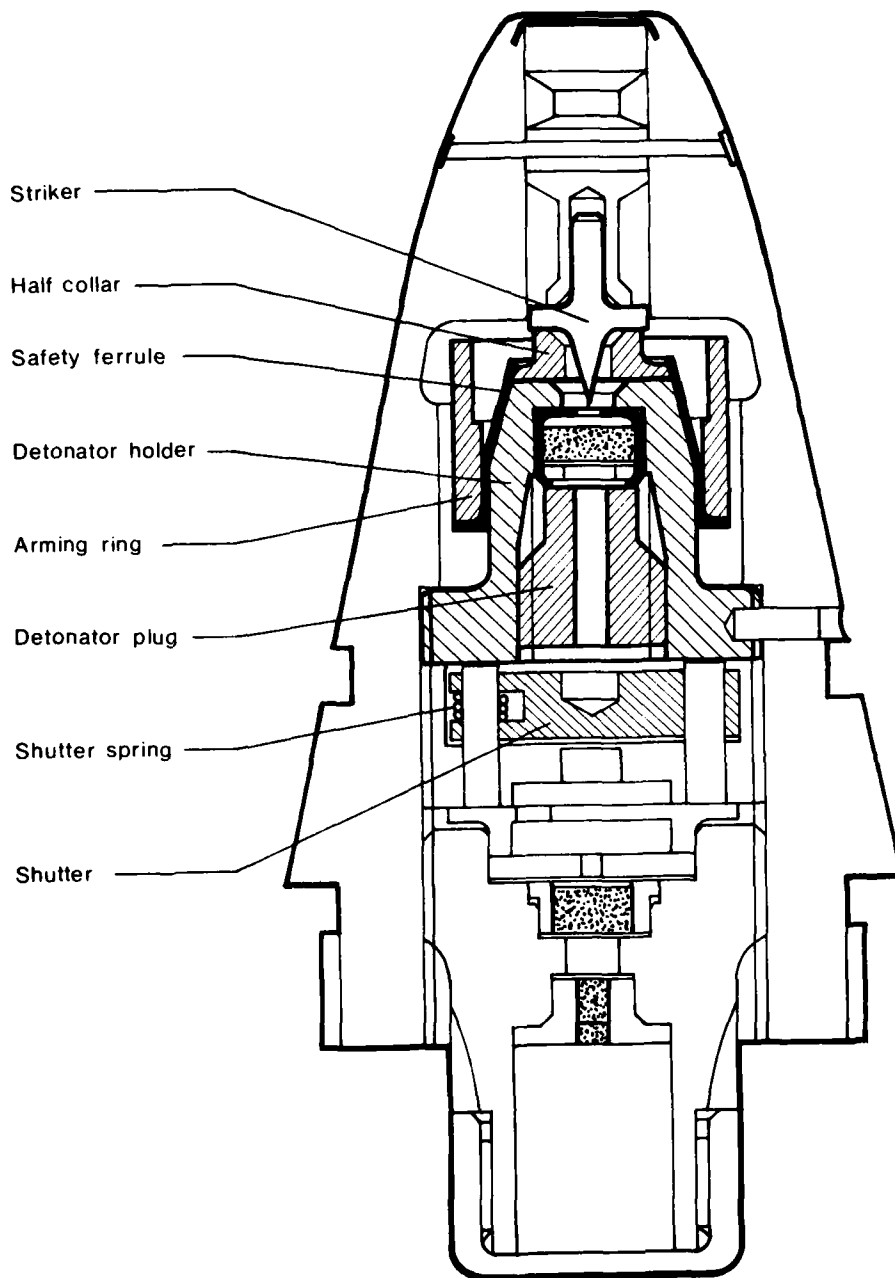
FIGURE 1 — Fuze No. 259 N4.
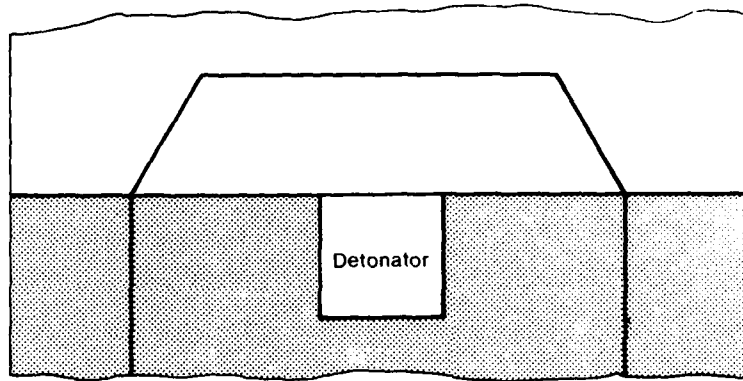
(a) FUZE A
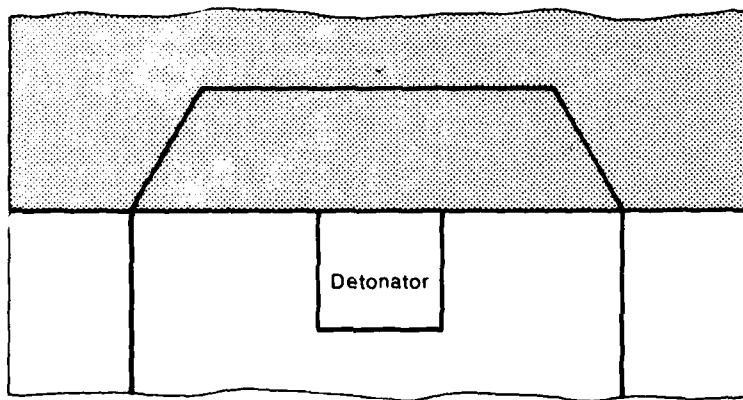
(b) STANDARD

FIGURE 2   Defect A - The arming ring is inverted.   This shows up as a
lighter grey area above the detonator compared to the standard
fuze, because the arming ring is thicker at the base.
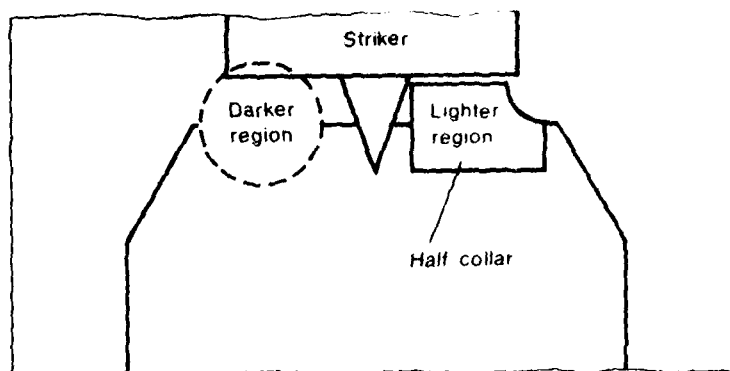
(a)   FUZE B (view 1)
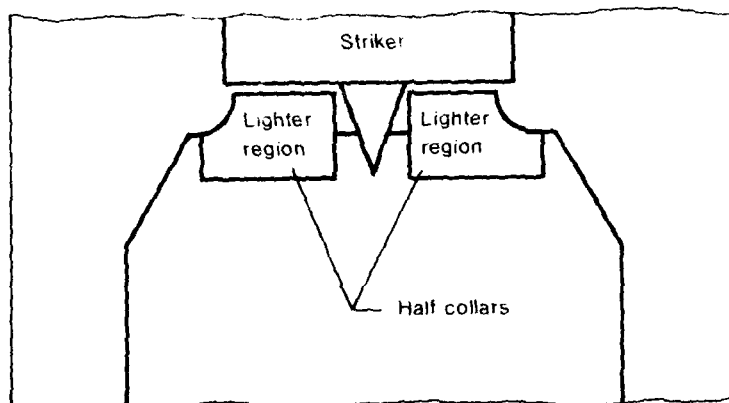
(b)   STANDARD

FIGURE 3   Defect B - One of two half collars is missing.   This is indicated
            by a darker grey area on one side of the striker point compared to
            the other side, above the level of the detonator.   The standard
            fuze has this area in a lighter grey colour on either side of
            striker, just above the detonator.
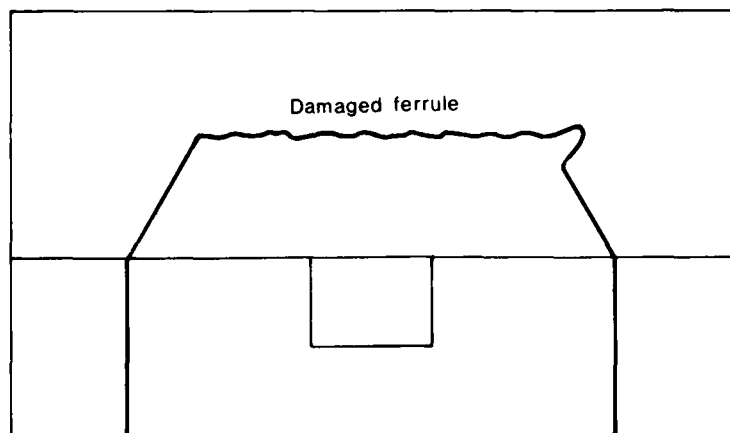
(a) FUZE C
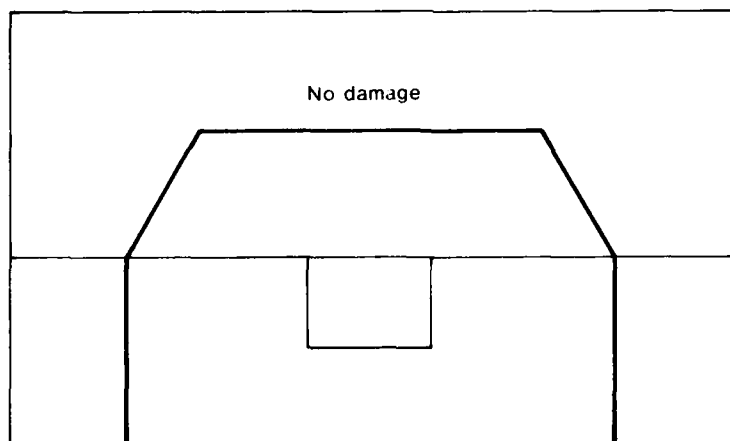
(b) STANDARD

FIGURE 4   Defect C - The safety ferrule is damaged.   The distortion at the
top of the ferrule as seen through the arming ring is obvious.
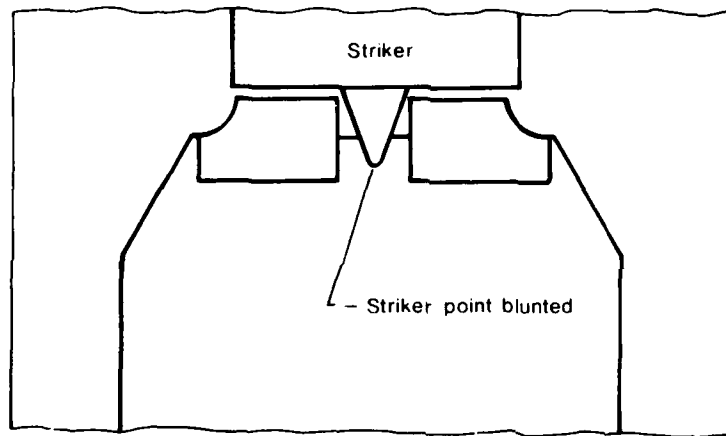
FIGURE 5   Defect D – The striker point has been blunted.   This cannot be
discerned readily when compared to the standard.

Hinge pin ─────

Shutter

Shutter
spring
missing

(a) FUZE E

Hinge pin ─────

Shutter
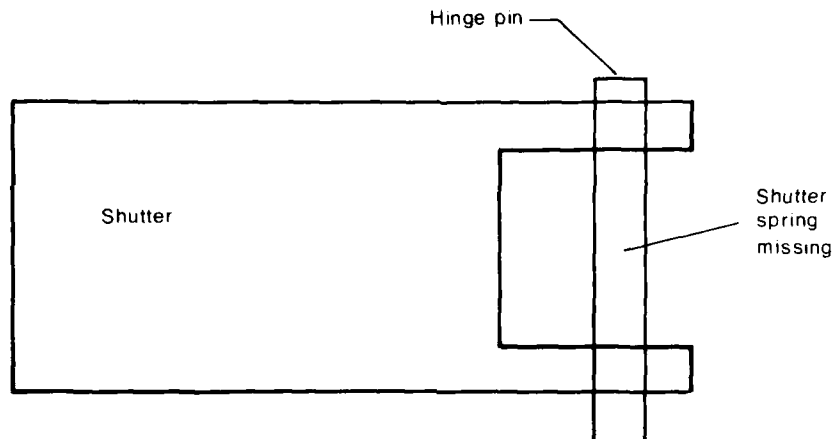
Shutter
spring
present
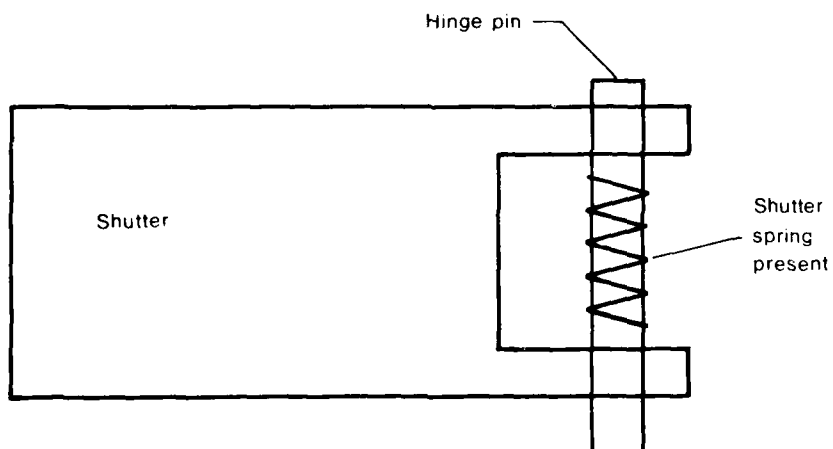
(b) STANDARD

FIGURE 6   Defect E - The shutter assembly spring is missing.   This is
clearly visible when comparing Fuze E with the Standard.   Note that
the shutter assembly is not oriented in any particular way.   This
is because it is not referenced to the fuze.

Detonator holder

Detonator plug

Dark area

Shutter

(b) FUZE F

Detonator holder

Detonator plug

Dark area

Shutter
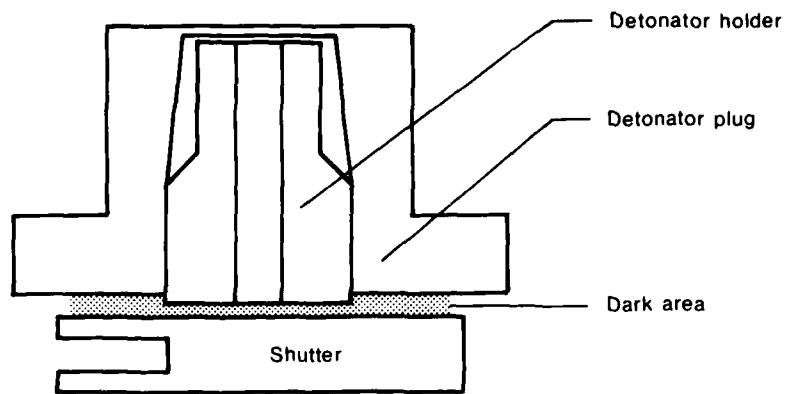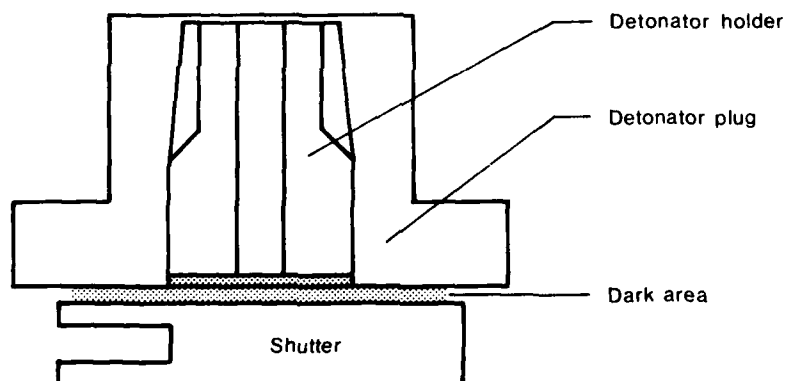
(b) STANDARD

FIGURE 7   Defect F - The detonator plug is not screwed fully home.   This
shows up as a lighter grey area below the base of the detonator
holder.   The image of the Standard show, in contrast, a dark area
into the base of the detonator holder indicating that the plug is
screwed fully home.
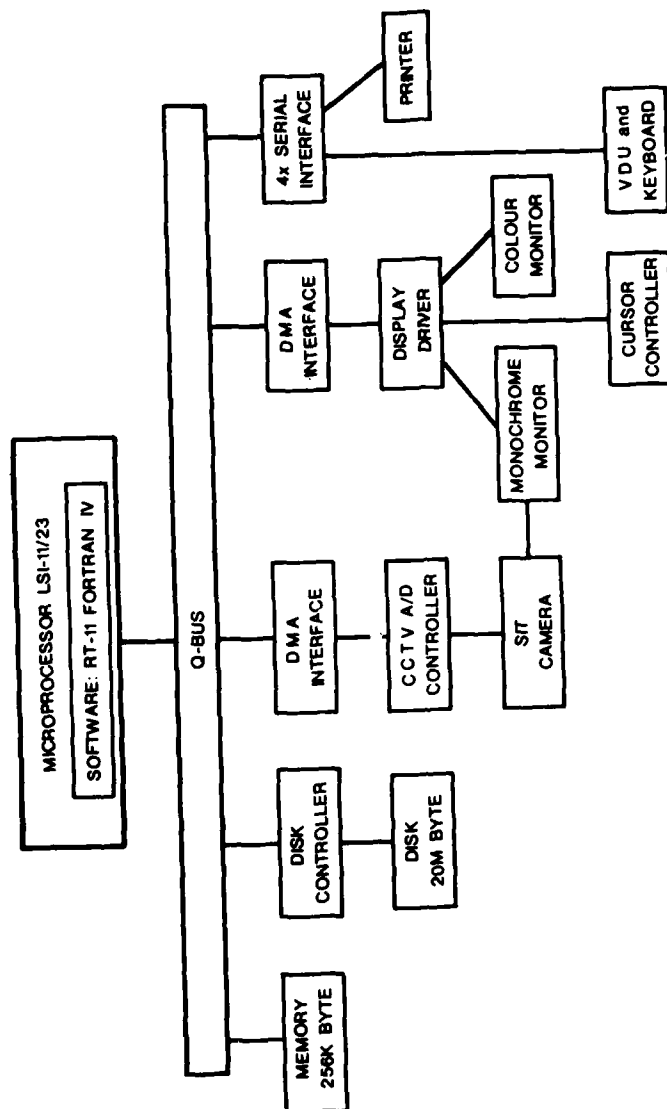
FIGURE 8   Block diagram of the system used for image acquisition, analysis and display.
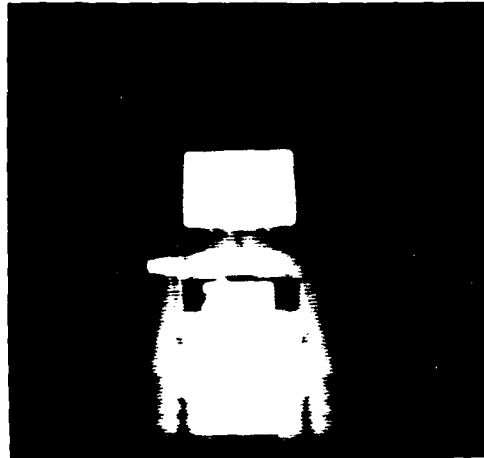
FIGURE 9   Image of Fuze No. 259.   The image is digitised into 256 x 256
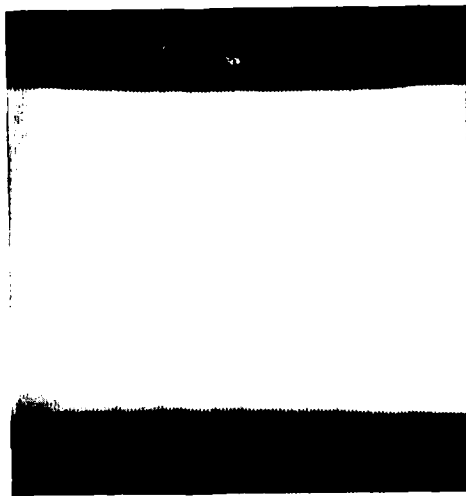pixels and 256 intensity levels.
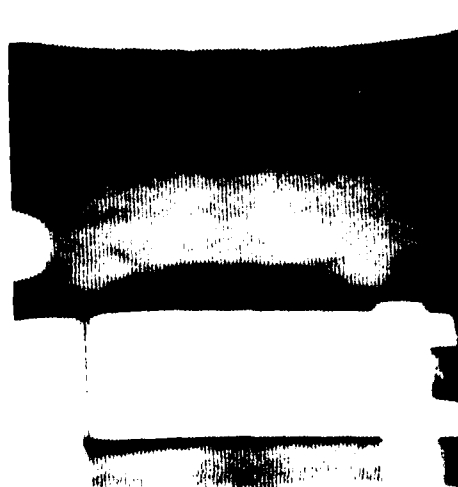
FIGURE 10   Image of a close-up view of the shutter assembly.
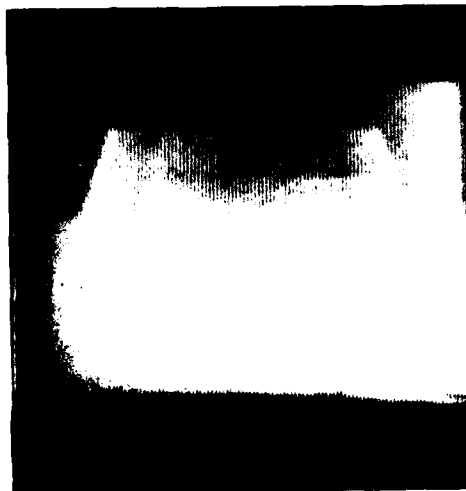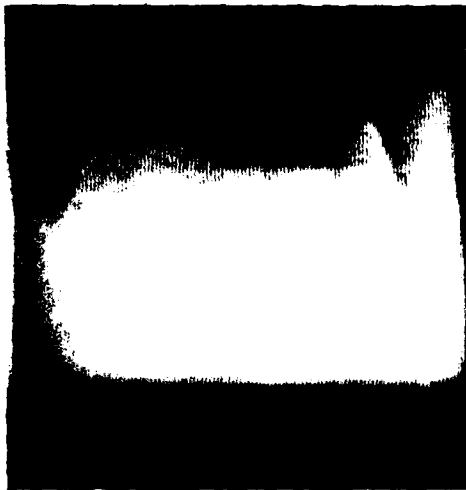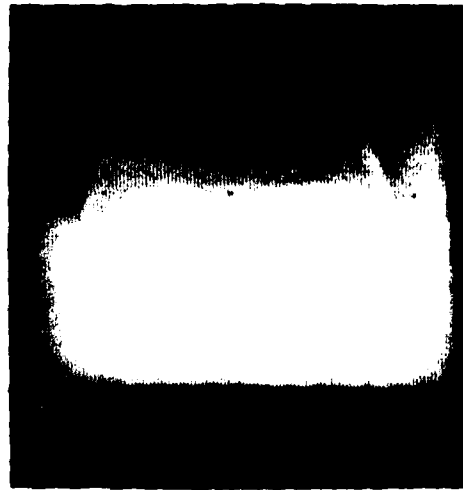
(a)

(b)

FIGURE 11   Image of the section containing the detonator, detonator holder,
             arming ring, half collars and the safety ferrule.   (a) Fuze A
             View 1 (inverted arming ring).   (b) Standard View 1.

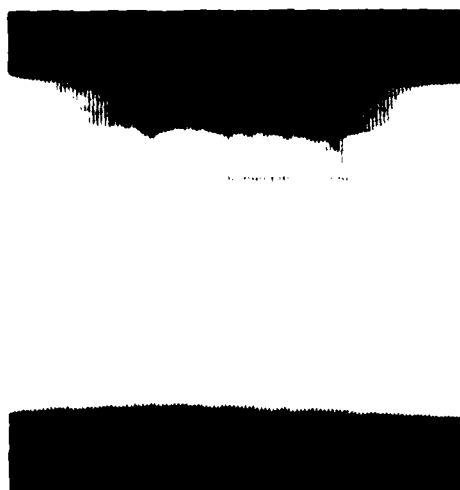(a)   (b)

(c)
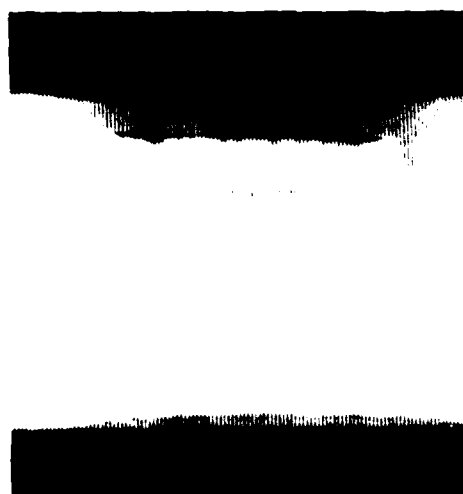
FIGURE 13   Images of the same section of fuze as shown in Figure 11.
             (a) Fuze B View 1 (half collar missing). (b) Fuze B View 2.
             (c) Standard.
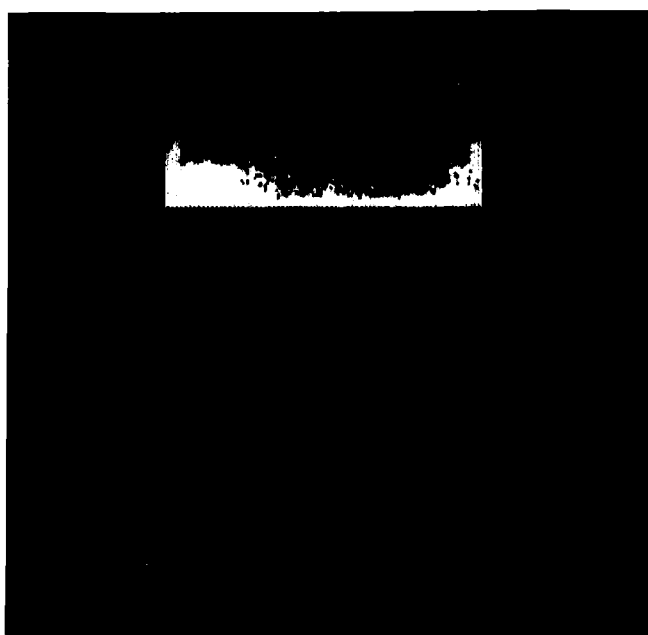
(a)   (b)

(c)

FIGURE 14   Images of Figure 13 with enhanced contrast inside the window.
(a) Fuze B View 1.   (b) Fuze B View 2.   (c) Standard.
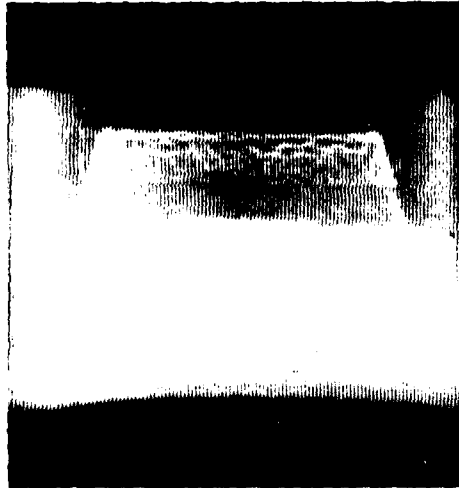
FIG. 15

(a)

(b)

FIGURE 16   Images of the same section of fuze as shown in Figure 11.
             (a) Standard.   (b) Fuze C (safety ferrule damaged).
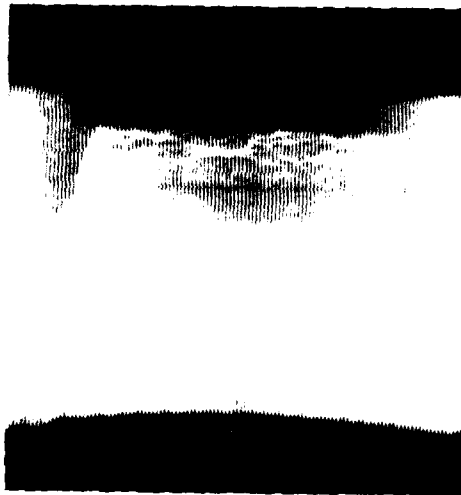
(a)

(b)

FIGURE 17   Images showing the edges of the safety ferrules in Figure 16
             after enhancement.

(c)
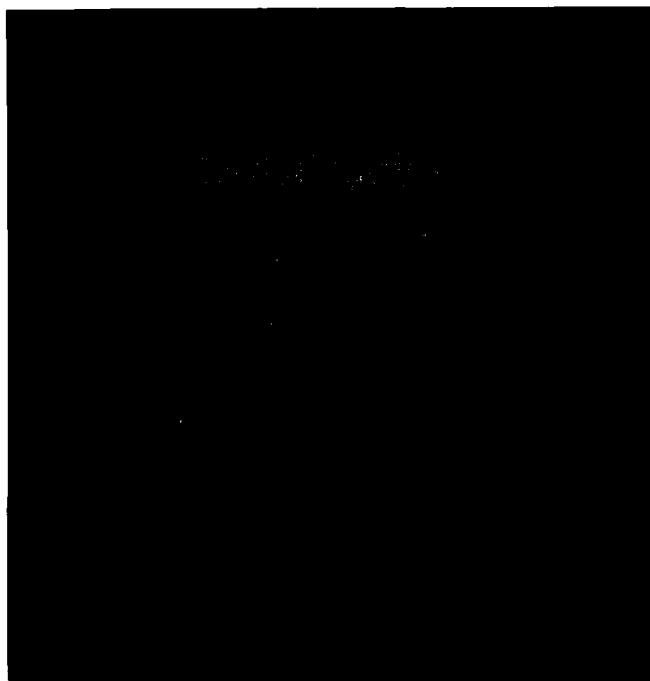
FIGURE 15   Images of Figure 13 displayed in pseudo colour.   Intensity
             levels above an appropriately chosen threshold are displayed in
             yellow inside the window, while those below the threshold are
             displayed in red.   (a) Fuze B View 1.   (b) Fuze B View 2.
             (c) Standard.   The Standard has less information in the
             intensity range displayed in red.

(a)
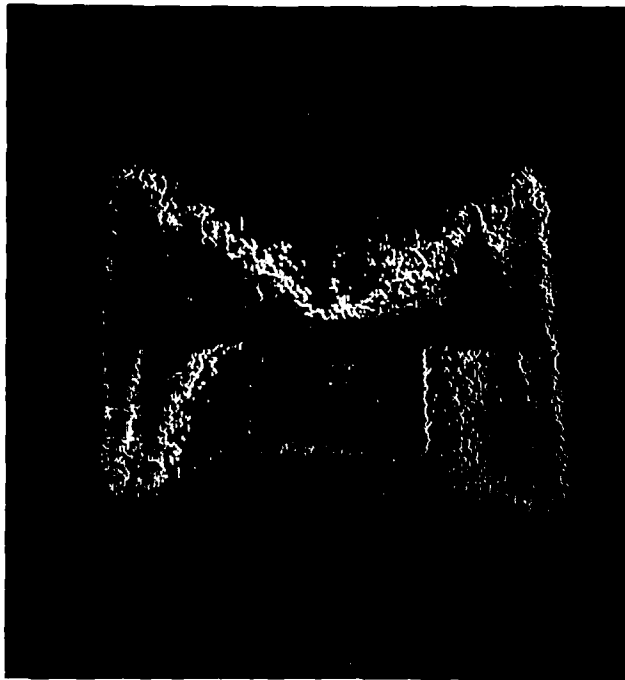
(b)
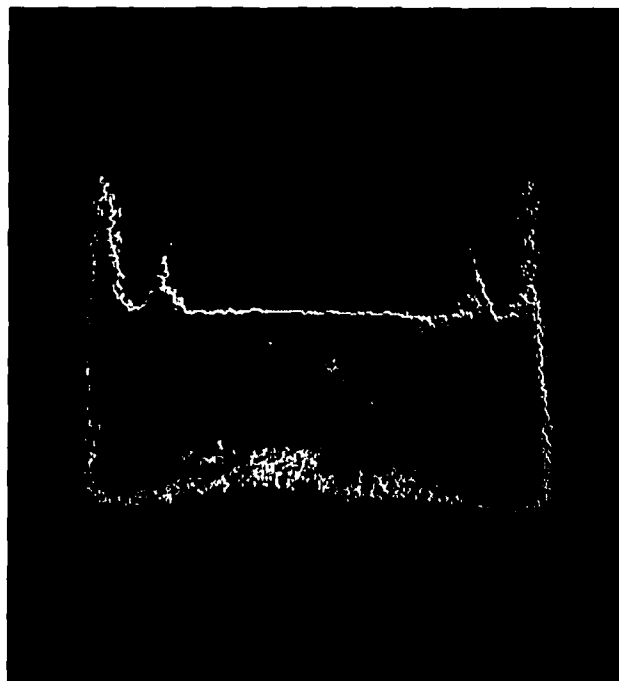
FIGURE 12   Images of Figure 11 displayed in colour.   Intensities above
              certain threshold are displayed in red.   (a) Fuze A View 1.
              (b) Standard View 1.
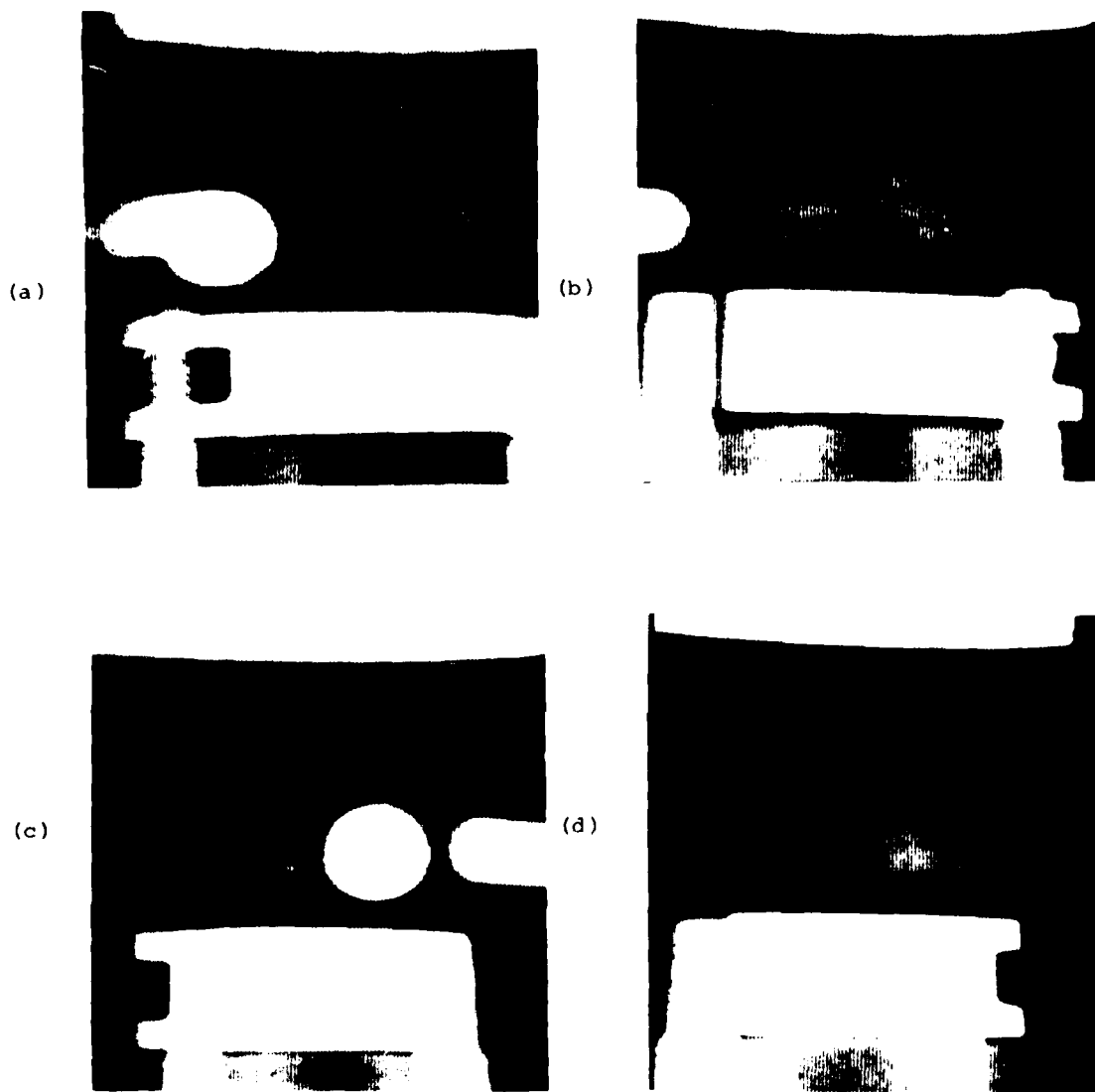
FIGURE 18   Images of shutter assembly.   (a) and (b) are respectively the
images of Fuze B View 1 and View 2, showing the presence of the
spring;   (c) and (d) are respectively the images of Fuze E View 1
and View 2, showing the spring missing.

FIG. 19

(a)
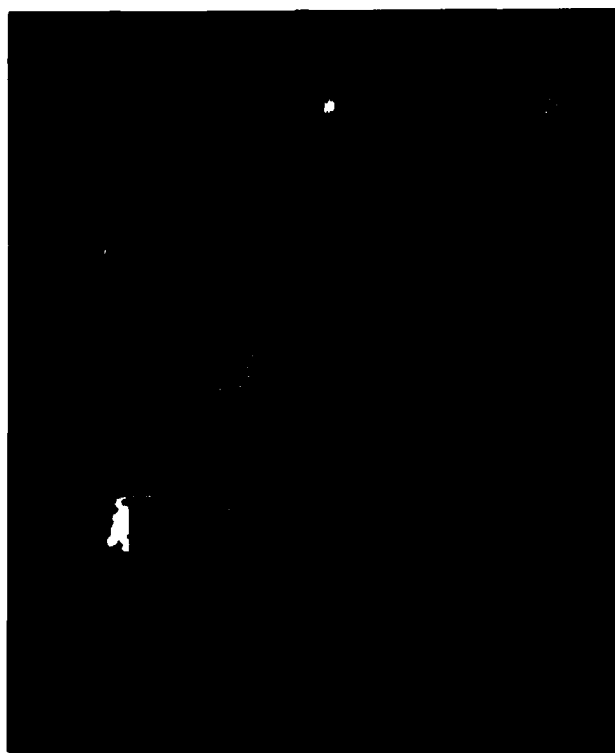
(b)

(c)

(d)

FIGURE 19   Images showing a small area in the vicinity of the springs of
             Figure 18 being processed to display intensity levels
             corresponding to that of the springs in yellow and the rest in
             red.
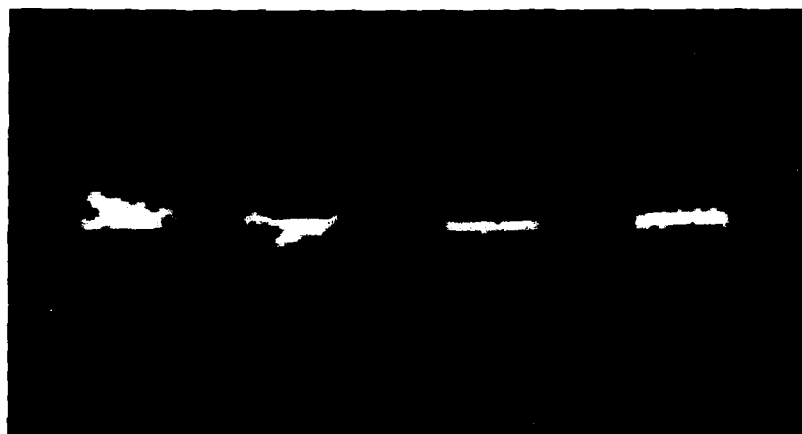
(a)   (b)   (c)   (d)

FIGURE 20   Images of the areas in the vicinity of the shutter springs extracted from Figure 19.   (a) and (b) are images with the spring, (c) and (d) are images with the spring missing.
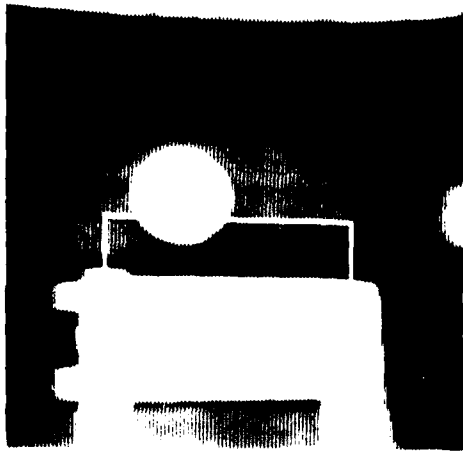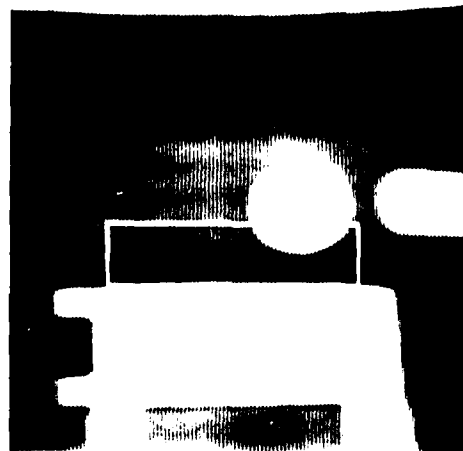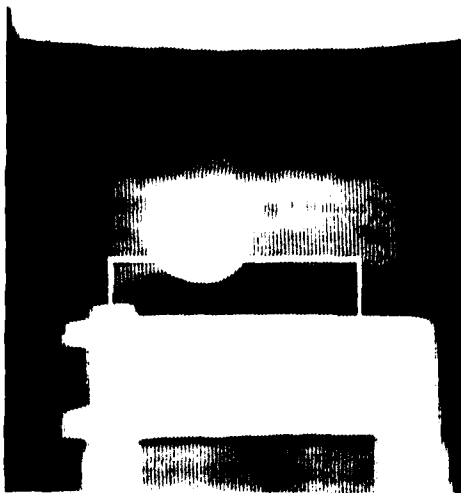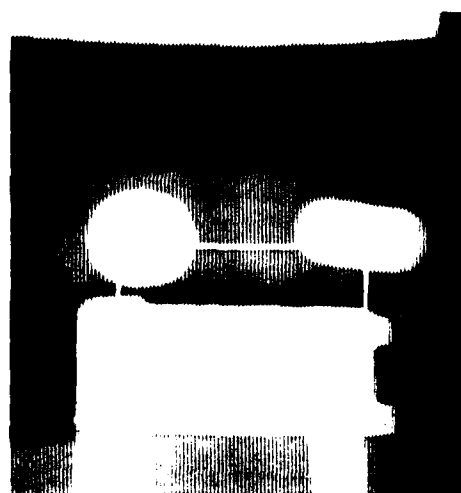
FIGURE 21   Images of the section fuzes showing the shutter, detonator holder
and the detonator plug.   (a) Fuze A.   (b) Fuze E.   (c) Fuze B.
(d) Fuze F (detonator plug not fully screwed home).

(a)

(b)

(c)

(d)
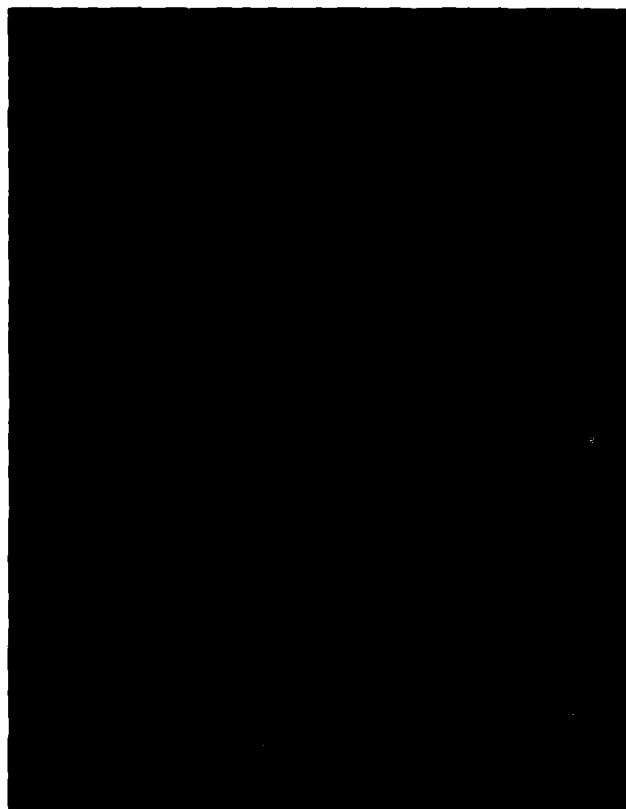
FIGURE 22   Images of the windows extracted from Figure 21 displayed in
             pseudo colour.   Intensity levels characterising the gap are
             displayed in purple.

(a)

(b)

(c)

(d)

FIGURE 23   Images of Figure 22 converted to the binary form.   The gaps are
             shown in white.

PERCENTAGE OF PIXELS BELOW THE THRESHOLD
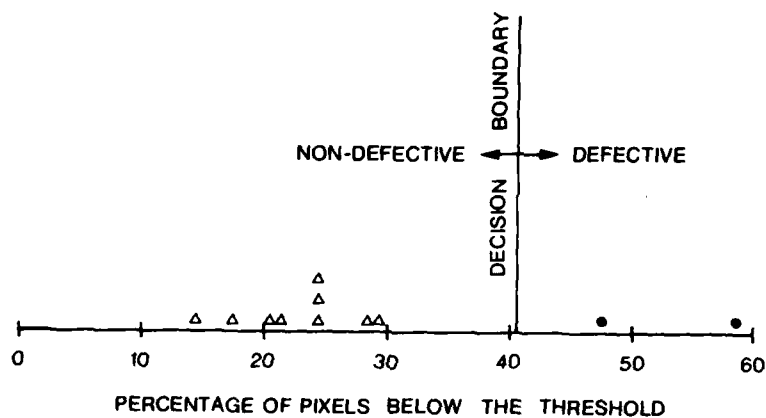
FIGURE 24   Identification of Defect B based on the percentage of pixels below a selected intensity threshold (information displayed in red in Figure 15).   △ denotes readings for non-defective fuzes and ● denotes readings for defective fuzes. The result indicates that one non-defective fuze has been identified as defective according to this classification.
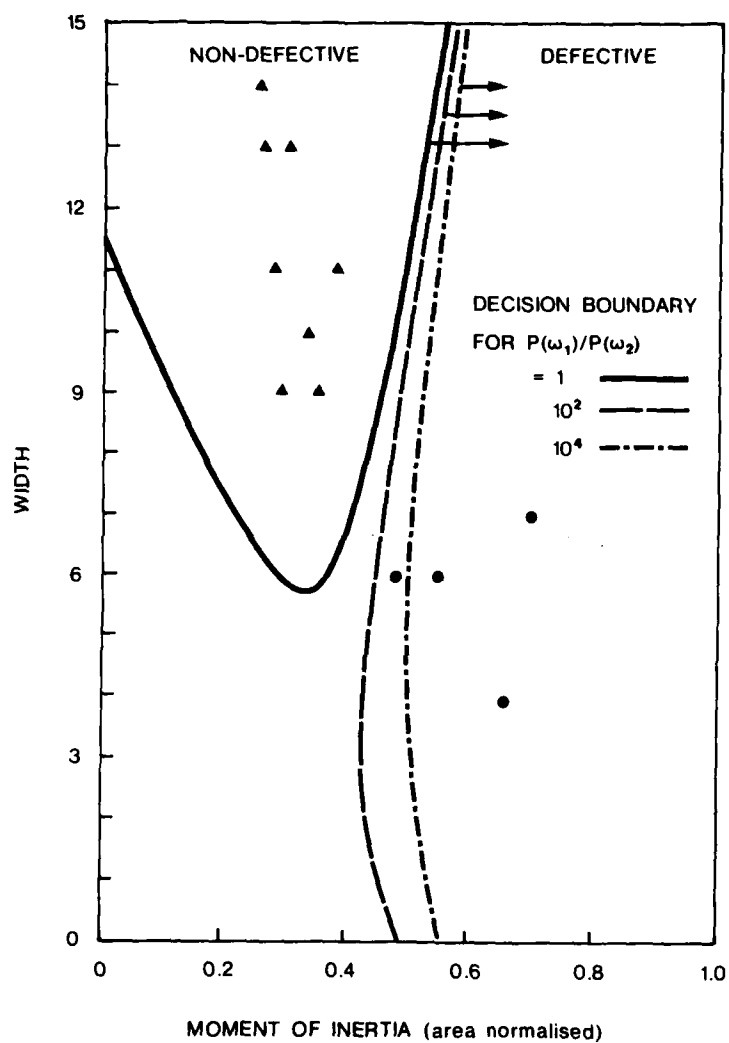
FIGURE 25   Identification of Defect E using the Bayes classifier. The
effect of a priori probabilities on the decision boundary is
illustrated. (▲ - non-defective fuze, ● - defective fuze. The
values are listed in Table 3).
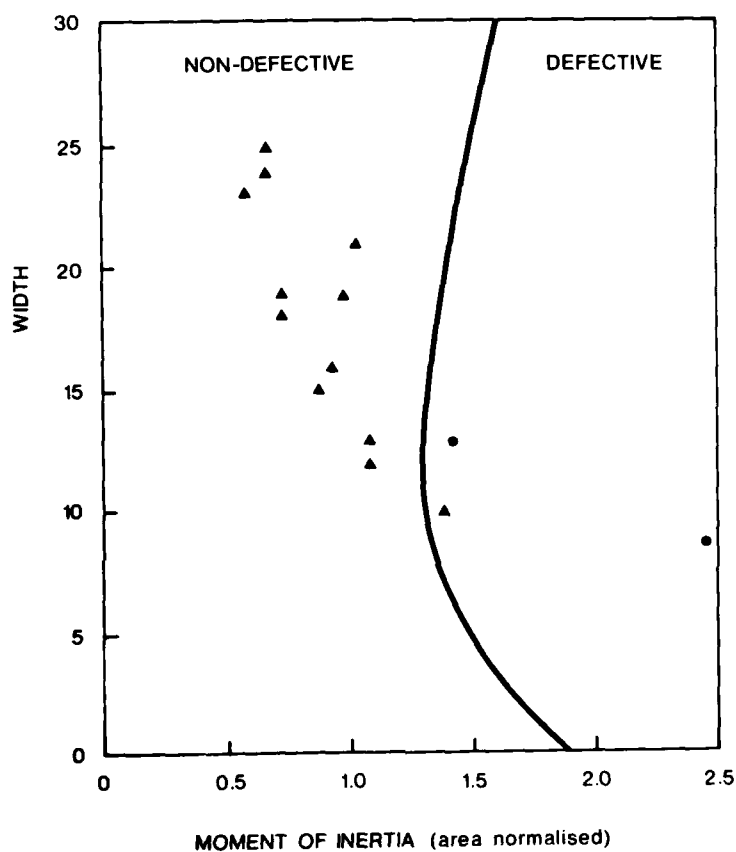
FIGURE 26   Identification of Defect F using the Bayes classifier. (▲ - non-
defective fuze, ● - defective fuze. The values are listed in
Table 4).

A N N E X

COMPUTER PROCESSING OF IMAGE DATA

The digital image processing for the study was performed using programs which were developed to enable interactive calculations on image data viewed on a video monitor. The programs were arranged so that all operations could be performed by a program written in FORTRAN IV calling subroutines from a specialised library. A flexible means of acquiring a digital image, processing it and interactively displaying both the acquired and processed image enabled a rapid evaluation of a number of image processing techniques. Control of the RAMTEK image display driver incorporates subroutines adopted from the manufacturer's firmware.

Two main methods of display were utilised on the RAMTEK whereby a display of 512 x 512 pixels comprised:

(i)   full screen or selectable and locatable portions there-of.

(ii) Sector based images of 256 x 256 PIXELS displayed in one of four sectors (numbered 1 to 4).

A brief outline of the image data processing software is given to indicate the general nature of processing required for image analysis techniques.

1   IMAGE ACQUISITION

All three programs place the HAMAMATSU camera under host computer control and digitize an analogue image to 256 grey levels and transfer it into Ramtek memory via host main memory.

GET   Single line scan 256 grey levels transferred to 1 of 4 specified sectors of the screen

INT   Similar function to GET, but the facility to integrate up to 256 frames. (noise reduction)

GET 512   Acquire a full 512 x 512 image and transfer to screen.

2.   IMAGE TRANSFER (SECTOR BASED)

CLR   Will clear specified sector by overwriting with the background level.

COP   Will copy from one sector to another as specified.

SAV   Will store on disk the image of a sector.

LOD   Will load from disk an image and display it in a specified sector.

ADD SUB Will add or subtract one full sector to OR from another and write into a third with provision for an off-set.

3.   WINDOW EXTRACTION AND INSERTION

WIN 1   A rectangular subarea or window of an image can be extracted from any part of the screen by addressing the starting and finishing co-ordinates with the cursor. The output is written onto disk as a file "win.out".

WIN 2　　Will read from disk the file "win.out" and write onto the screen at a starting address specified by the cursor. A magnification factor can be entered from the keyboard.

WIN 3　　Is a version of WIN 1 which allows the cursor address points to be written onto the terminal screen before transmitting the final address to the Ramtek for window extraction.

WIN 4　　Is a version of WIN 2 which similarly allows address points to be written at the terminal before transmitting to the Ramtek for window insertion.

All four of these programs have the option to address points directly as X and Y values entered at the keyboard.

4.　IMAGE DISPLAY CONTROL

GREY　　Loads a video look-up table which generates 256 grey level signals for a monochrome display from corresponding pixel values (Z) stored in RAMTEK memory.

LEV 12　　Loads a video look-up table for a colour display based on a color spectrum from blue (Z = 0) to magenta (Z = 256). Each colour is a graduated mixture of two primary colours. Low Z comprises blue and green, intermediate Z comprises green and red and high Z comprizes red and blue.

The program optionally accepts an upper and lower threshold value from the keyboard to produce a binary image. The pixel values within the range are displayed in green and all others are in black (i.e. not visible).

LEV 20　　Allows the setting of any range of pixels to any colour. Ranges and colour levels are entered from the keyboard. A colour table can therefore be built up interactively.

SELECT　　This program allows the interactive selection of a video look-up table based on the spectrum of LEV 12.

The position of the cursor on a reference spectrum displayed on the monitor determines the colour assigned to a pixel with the value $\emptyset$. A wrap around effect is employed on the spectrum so that the colours for all the values up to 256 are changed as the cursor is moved along the reference.

This program is particularly useful for examining quickly the detail spread through the image.

5. <u>IMAGE PROCESSING</u>

HIST GY   Allows cursor selection of a window of image and plots a
          histogram of its pixel values on a set of axis on the display
          screen.

          The cursor can then be used to select a range from the
          histogram. The pixel values of the window of image within this
          range are then expanded out to cover 256 grey levels. These
          values overwrite the original window.

LEV SET   A window of image is firstly selected by cursor entry. A
          threshold is then set at the keyboard which displays the window
          as a binary image.

          Different thresholds can be input at the terminal to change the
          constitution of the binary image. The image outside the window
          is unaffected.

SMOOTH   This program operates on 3 x 3 windows centred on each pixel and
          its four diagonal neighbours. The most homogeneous window is
          selected and the original centre pixel is replaced by the
          average of the nine values in the selected window. This method
          tends to reduce noise while sharpening edges.

TEMNOR   Takes a 3 x 3 neighbourhood centred on each pixel and performs a
          dot product with a selected 3 x 3 template. The centre pixel is
          then replaced by the sum of the dot products.

          The following templates are available and can be selected at run
          time:

PNT :				VFT :		
-1	-1	-1		-1	2	-1
-1	-8	-1		-1	2	-1
-1	-1	-1		-1	2	-1

HOL :				HGT :		
-1	-1	-1		1	2	1
2	2	2		0	0	0
-1	-1	-1		-1	-2	-1

RHS :				LHS :		
2	-1	-1		-1	-1	2
-1	2	-1		-1	2	-1
-1	-1	2		2	-1	-1

VGT :				W1V :		
1	0	-1		1	$\sqrt{2}$	1
2	0	-2		0	0	0
1	0	-1		-1	$-\sqrt{2}$	-1

W2V :				W3V :		
1	0	-1		0	-1	$\sqrt{2}$
$\sqrt{2}$	0	$-\sqrt{2}$		1	0	1
1	0	-1		$-\sqrt{2}$	1	0

W4V	:	$\sqrt{2}$	-1	0		W5V	:	0	1	0
		-1	0	1				-1	0	-1
		0	1	$-\sqrt{2}$				0	1	0
W6V	:	-1	0	1		W8V	:	-2	1	-2
		0	0	0				1	4	1
		1	0	-1				-2	1	-2
W7V	:	1	-2	1		W9V	:	1	1	1
		-2	4	-2				1	1	1 (÷9)
		1	-2	1				1	1	1

OPTIONS

INP : Allows entry of user specified template values from the keyboard.

ESP : Square root of sum of squares of the results of the four templates W1V, W2V, W3V, W4V applied in turn.

LSP : The same procedure using templates W5V, W6V, W7V, W8V.

GRA : Horizontal and vertical detection of gradients.

NOA : Normalise - stretch image accross 256 levels.

SQW : Squeeze image.

DIL : Dilate image.

All options operate on user specified windows of image selected by cursor.

6. IMAGE SEGMENTATION AND FEATURE EXTRACTION

The following programs contain the image analysis algorithms and are used in this sequence:

GFT   To acquire an image from the camera and place into sector 2. Any reference background is placed in sector 1.

LFV   To set thresholds for a binary image.

SBR   Subtracts from sector 2 the background in sector 1 and, with an off-set, displays the result in sector 3.

        This operation determines the run encoded values of the binary image set by LFV.

ANB   Analyses the image in sector 3 resulting from the operation of LFV and SBR.

        The features of the objects detected are extracted (perimeter, area, centroid, etc.) and printed out on a table.

REP   Will automatically repeat the sequence GET, SBB, ANB using the previously set thresholds in LEV.

ANA   Will analyse an image in any sector by reading each pixel in turn after LEV has been used to set a threshold. Because this option does not use run encoded image data, the feature extraction is much slower than option ANB with SBB

7. UTILITIES

VECTOR   Will draw a line between any two co-ordinates entered at the keyboard. The "pen" can be lifted and drawn at different FOREGROUND values. The actual color depends on the color table loaded at the time by LEV 20.

TEXT   Will write standard ASCII text onto the display. The position is specified by cursor and a magnification factor can be entered from the keyboard.

PROF   Will plot the intensity profile of a line section of image on the display. The section is parallel to the x-axis and is selectable using the cursor. Subsequent profiles can be plotted on the same axis for comparison.

PROF S   Is a self incrementing version of PROF which will scan through a specified section of image line by line. A profile of the section will be built up on the set of axis on the screen.

AVER 1   Will accept from keyboard or cursor a specified portion of image and calculate the average value of all pixels in that portion.

AVER 2   Will calculate the average values of two specified portions of image. The window of higher value will be overwritten in red FOREGROUND and the lower in green (background). This program is useful for highlighting adjacent areas of different intensities.

HIST 4   Will take the output image (WIN.OUT) of window extraction programs WIN 1 and WIN 3 and produce a histogram of pixel values.

An output table (HIST.OUT) contains the histogram together with a mean and standard deviation.

VALL   Allows the selection of single pixel points by cursor. The value and co-ordinates are typed at the terminal.

DISTRIBUTION LIST

MATERIALS RESEARCH LABORATORIES

    Director
    Superintendent, Physics Division
    Dr D.W. Williams
    Library   (2 copies)
    Dr K.K. Wu
    Mr J.D. Quinn
    Mr D.F. Hedger

DEPARTMENT OF DEFENCE

    Chief Defence Scientist (for CDS/DCDS/CERPAS)   (1 copy)
    Army Scientific Adviser
    Air Force Scientific Adviser
    Officer-in-Charge, Document Exchange Centre   (18 copies)
    Technical Reports Centre, Defence Central Library
    Director of Quality Assurance Support (DQAS)
    Assistant Director, Defence Scientific and Technical Intelligence,
        Joint Intelligence Organisation
    Librarian, Bridges Memorial Library
    Librarian, Engineering Development Establishment
    Defence Science Adviser   (Summary Sheets Only)
        Australia High Commission, London
    Counsellor Defence Science, Washington, D.C.   (Summary Sheets Only)
    Librarian, (Through Officer-in-Charge), Materials Testing
        Laboratories, Alexandria, NSW
    Senior Librarian, Aeronautical Research Laboratories
    Senior Librarian, Defence Research Centre Salisbury, SA
    Head, Office of Defence Production
    Head of Staff, British Defence Research & Supply Staff (Aust)

OTHER FEDERAL AND STATE DEPARTMENTS AND INSTRUMENTALITIES

    NASA Canberra Office, Woden, ACT
    The Chief Librarian, Central Library, CSIRO
    Library, Australian Atomic Energy Commission Research Establishment

MISCELLANEOUS - AUSTRALIA

    Librarian, State Library of NSW, Sydney NSW
    University of Tasmania, Morris Miller Lib., Hobart, Tas.

DISTRIBUTION LIST
(Continued)

MISCELLANEOUS

Library - Exchange Desk, National Bureau of Standards, USA
UK/USA/CAN/NZ ABCA Armies Standardisation Representative   (4 copies)
Director, Defence Research Centre, Kuala Lumpur, Malaysia
Exchange Section, British Library, UK
Periodicals Recording Section, Science Reference Library,
    British Library, UK
Library, Chemical Abstracts Service
INSPEC: Acquisition Section, Institute of Electrical Engineers, UK
Engineering Societies Library, USA
Aeromedical Library, Brooks Air Force Base, Texas, USA
Documents Librarian, The Centre for Research Libraries, Chicago Ill.
Defense Attache, Australian Embassy, Bangkok, Thailand
Library, Department of Scientific and Industrial Research
    Wellington, NZ